Model Studies of Catechol Dioxygenases. Important Role of Monodentate Catecholate-Iron(III) Intermediate

Satoshi FUJII, Hiroaki OHYA-NISHIGUCHI,*,†† Noboru HIROTA, and Akira NISHINAGA†
Department of Chemistry, Faculty of Science, Kyoto University, Sakyo-ku, Kyoto 606
†Department of Applied Chemistry, Osaka Institute of Technology, Ohmiya 5, Asahi-ku, Osaka 535
(Received December 11, 1992)

The catechol dioxygenase model reactions of three model systems have been investigated by EPR, optical, and electrochemical studies. In each model system, some kinds of intermediates could be detected by EPR and optical spectroscopies. The intermediate structures and the reaction times suggest that the monodentate catecholate complexes play an important role in the catalytic cycle. Based on the EPR spectra obtained aerobically and anaerobically, iron(III)-monodentate dianionic catecholate is the O_2 reactive species for Fe(nta)(nta=nitrilotriacetato) and Fe(sal-L-aa)Cl (sal-L-aa=*N*-salicylidene L-amino acidato) systems and iron(II)-semiquinonate for Fe(salen)Cl (salen=*N*,*N*′-ethylenebis(salicylideneaminato) system. Electrochemical data suggest that this electron transfer in Fe(salen)Cl system is caused by the ligand distortion. The catecholate(sal-L-val)iron(III) complex reacted with dioxygen to yield the ring cleavage products (ca. 80%). On the basis of the observations, the novel reaction mechanism of the Fe(sal-L-aa)Cl system having mainly monodentate catecholate intermediate, is proposed. Finally, the correlation between the coordination environments of non-heme iron(III) complexes and EPR parameters is discussed.

Catechol dioxygenases (CTD), non-heme iron enzymes, catalyze the intradiol cleavage of catechol to *cis*,*cis*-muconic acid by dioxygen[1,2] and serve as central enzymes for degrading aromatic compounds. Protocatechuate 3,4-dioxygenase (PCD), one of the most characterized of this group, has an active site consisting of trigonal bipyramidal high-spin iron(III) center coordinated to two tyrosines (one equatorial, the other axial), two histidines (one equatorial, the other axial), and a water (equatorial).[3] The proposed reaction mechanism involves initial substrate (S) binding to the iron(III) center of the enzyme (E), followed by the attack of dioxygen on the enzyme-substrate complex (ES). The enzyme-substrate-dioxygen complex (ESO_2) formed is converted to ESO_2^* and then yields the oxygenation products (P) (Scheme 1).[4] Mössbauer[5—7] and stopped-flow-kinetic[4,8] studies indicate that the iron remains in a high-spin iron(III) state throughout the course of the reaction. However, the details of the mechanism have not been clarified yet. Two important problems to be solved for clarifying the reaction mechanism are as follows: First, does the valence of iron change during the catalytic cycle? Second, which intermediate does the molecular oxygen attack?

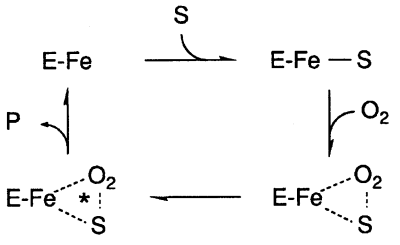

Scheme 1.

A number of studies using both enzymes and model complexes have been made to clarify the reaction sequence and some reaction mechanisms have been proposed.[9—13] Especially, the results of model studies are important. Que and co-workers[14] proposed the mechanism involving the iron(III)(L)-catecholate intermediate (L: tripodal ligands). However, Funabiki and co-workers[15] proposed the iron(II)-semiquinone intermediate on their $FeCl_3$/bpy/py system. Recently, Que and co-workers also proposed the iron(II)-semiquinone intermediate on their Fe(bpg) (bpg=*N*,*N*-bis(2-pyridylmethyl)glycinato)[12] and Fe(tpa) (tpa=tris(2-pyridylmethyl)amine)[16]/3,5-di-*t*-butylcatechol (H_2dbc) systems.

We have investigated the model reaction of Fe(nta) (nta=nitrilotriacetato) and Fe(salen)Cl (salen=*N*,*N*′-ethylenebis(salicylideneaminato) with catechols by EPR and optical spectroscopies.[17] On the basis of the observations, we reported that the valence change of iron depends on the used ligand and that the species attacked by dioxygen is of monodentate catecholate losing both its OH protons.

In the present paper, we have extended our model studies to Fe(III) complexes of *N*-salicylidene L-amino acids, Fe(sal-L-aa)Cl (aa: ala, val, phe, his) (Scheme 2).[18] Since the coordination geometry and the types of ligands(nitrogen/oxygen) differ with used L-amino acids (type **1**: ala, val, phe; type **2**: his) and with nta and salen, the effects of the geometry and the ligand type can be considered. Moreover, containing L-amino acids in the ligands, these complexes are expected to afford the enzyme-like condition to the iron. Indeed, these complexes react with catechols much faster than nta and salen complexes. In the Fe(sal-L-aa)Cl system, there was no apparent evidence for the iron(III)

††Present address: Institute for Life Support Technology, Yamagata Technopolis Foundation, Numagi 683, Yamagata 990.

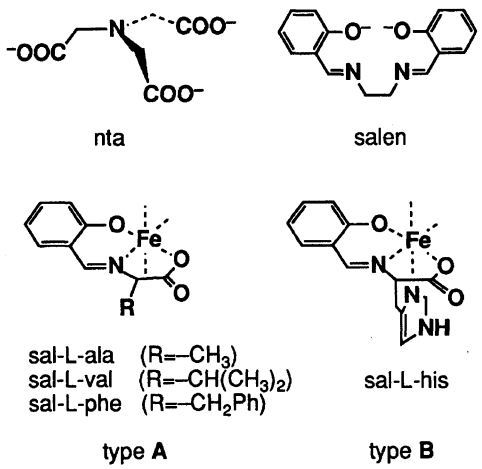

Scheme 2.

ion to be reduced, and no signal of radical could be observed. Additonally, the ratio of the dianionic monodentate catecholate intermediate to other intermediates having other coordination mode of catecholate is relatively high. These observations suggest that the charge and spin state of iron are unchanged throughout the reaction and that dianionic monodentate catecholate complex is a key intermediate. A comparison of the spectroscopic and reactive properties of these three model systems (nta, salen, and sal-L-aa) gives useful insights into the reaction mechanism for the enzymes.

In this study, we determined the intermediate structures mainly with the EPR parameters. As for the heme enzymes and the model heme complexes which have a common porphyrin ligand, their axial ligands can be deduced from the parameters tetragonality and rhombicity calculated from the observed g values. On the other hand, such a relation has not been reported in the cases of non-heme iron enzymes and complexes. Therefore, it is expected to find a relation between the EPR parameters and the coordination environments of non-heme iron(III) enzymes and complexes. Finally, we discuss a correlation between the coordination environments of the non-heme iron(III) complexes and their EPR parameters, which we found through the course of our studies.

Experimental

Materials. H_2dbc and pyrocatechol (H_2cat) were recrystallized from hexane and toluene solution, respectively. 3-Methylcatechol (3MeH_2cat) and 4-methylcatechol (4MeH_2cat) were sublimed under reduced pressure. 4-*t*-Butylcatechol (H_2pbc), 3,4-dihydroxybenzoic acid (protocatechuic acid; H_2pca), 3,4-dihydroxyphenylacetic acid (homoprotocatechuic acid; H_2hpca), 4-nitrocatechol (4NO_2H_2cat) were used as received. All other reagents and solvents were of the highest quality commercially available and used without further purification.

Fe(nta)$(H_2O)_2$,[14] Fe(salen)Cl,[19] and Fe(sal-L-aa)Cl[18] were synthesized according to published procedures.

Sample Preparation. All the samples were prepared under both air and degassed conditions. The sample solutions of Fe(nta) were prepared by mixing Fe(nta)$(H_2O)_2$ (2 mM, 1 M=1 mol dm^{-3}) and catechols, the molar ratios being 1 : 1, 1 : 10, and 1 : 100, respectively, in an aqueous borate buffer (1 part) and DMF (2 part) solution. The use of the borate buffer was to prevent the autoxidation of catechols.[10] The sample solutions of Fe(salen)Cl were prepared by dissolving [Fe(salen)Cl]$_2$ and H_2dbc followed by the addition of potassium *t*-butoxide (*t*-BuOK). The sample solutions of Fe(sal-L-aa)Cl were prepared by mixing Fe(sal-L-aa)Cl and H_2dbc in an 1 : 1 molar ratio in MeOH. In order to generate selectively monoanionic catecholate, Hdbc$^-$, or dianionic catecholate, dbc^{2-}, 1 equiv or 2 equiv of *t*-BuOK was added to the mixture.[18] The oxygenation was carried out under air at room temperature for EPR and optical measurements. In the salen and the sal-L-aa systems, only H_2dbc was used as the substrate, because it exhibits good reactivity for the nta system.

In this study, product analysis was performed only with the Fe(sal-L-val)Cl system because of fast reaction. Typically, 0.2 mmol of the complex, 2 mmol of H_2dbc, and 2 mmol of *t*-BuOK were reacted in 10 mL of MeOH in an oxygen atmosphere at 10 °C for 48 h. After the reaction was completed, the organic products were extracted with CH_2Cl_2. The products were separated by preparative chromatography on a silica gel plate being developed with CH_2Cl_2.

Physical Measurements. EPR spectra were recorded on a JEOL FE-3X X-band spectrometer at 4.2 and 77 K. Cr(III) in MgO (g=1.9800) was used as a standard g marker. UV-visible spectra were obtained on an Ohtsuka Electronic Co., Ltd. MCPD-1000 28C spectrophotometer, with which EPR and optical spectra can be measured simultaneously for the same sample in a same quartz tube. Electrochemical measurements were made in Me_2SO with 0.1 M tetra-*n*-butylammonium tetrafluoroborate as an electrolyte on a PAR Model-173 potentiostat using a Au working electrode, a Au counter electrode, and a Ag^+/Ag reference electrode. Ferricinium/ferrocene couple was used as an internal standard (calibrated +400 mV vs. NHE). NMR spectra were obtained in $CDCl_3$ and were recorded on a Varian Unity 300 spectrometer.

Results

EPR and Optical Studies. Almost all the complexes appeared in the model reactions are high-spin iron(III) complexes. EPR spectra of high-spin iron(III) are generally analyzed by the following S=5/2 spin Hamiltonian:

$$\mathcal{H} = D[S_z^2 - 35/12] + E[S_x^2 - S_y^2] + g_o\beta \boldsymbol{H}\cdot\boldsymbol{S} \qquad (1)$$

The ground state for high-spin d^5 system is sixhold degenerate ^{6}S. The zero field splitting terms partly lift the degenaracy and the sextet results in three Kramers doublets. It is well-known that the observed g values depend upon the parameter E/D only, if $|D|$, $|E| \gg g\beta H$ (ca. 0.3 cm^{-1} for X-band). From our numerical calculations of eigenvalues of Eq. 1, the observed g values show slight changes when $|D| > 0.4$ cm^{-1} (this condition is fulfilled for the complexes used in this study).

Therefore, we can evaluate the E/D easily from the observed g values (Fig. 1). The E/D value is a measure of the distortion of the electronic environment of the iron ion. The species with different E/D are, hence, expected to have different environments.

In this paper, we investigate the structures of the intermediate catecholate complexes. The possible coordination modes of catecholate are following three types: Type I; monodentate $Hcat^-$, Type II; didentate cat^{2-}, Type III; monodentate cat^{2-} (Scheme 3).

Fe(nta) System. Fe(nta) exhibits a typical EPR spectrum of a high-spin non-heme iron(III) system ($g=$ 9.6 and 4.3; $E/D\approx1/3$). Upon addition of catechols, the color of the solution changed and new EPR signals appeared due to the formation of the didentate catecholate complex. EPR spectra of some catecholate complexes, shown in Fig. 2, are almost the same despite the difference of the substrate catechols. Similar spectra were reported by Cox et al.[20] The value of E/D corresponding to the chelated catecholate species is ca. 0.20 (Table 1). The sharp signal at $g=4.3$ in each spectrum corresponds to Fe(nta) uncoordinated by catecholate.[21]

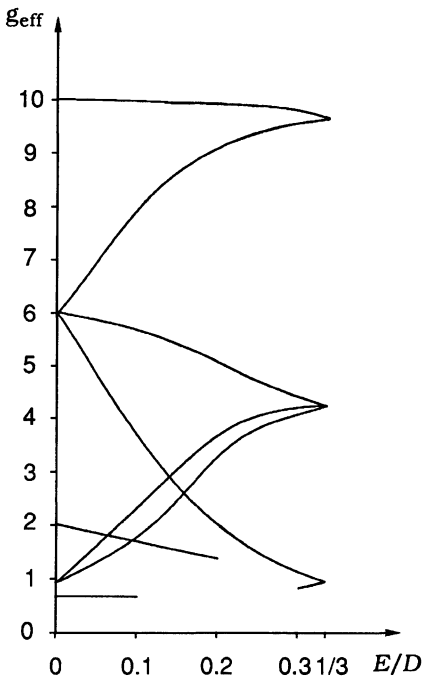

Fig. 1. The effective g values for the $S=5/2$ spin Hamiltonian plotted against E/D. This diagram shown is calculated with $D=1.0$ cm^{-1}.

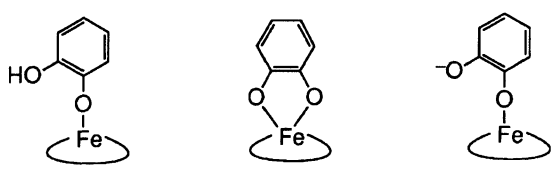

Scheme 3.

It is noted that only dbc complex showed an EPR spectrum derived from two species among the complexes

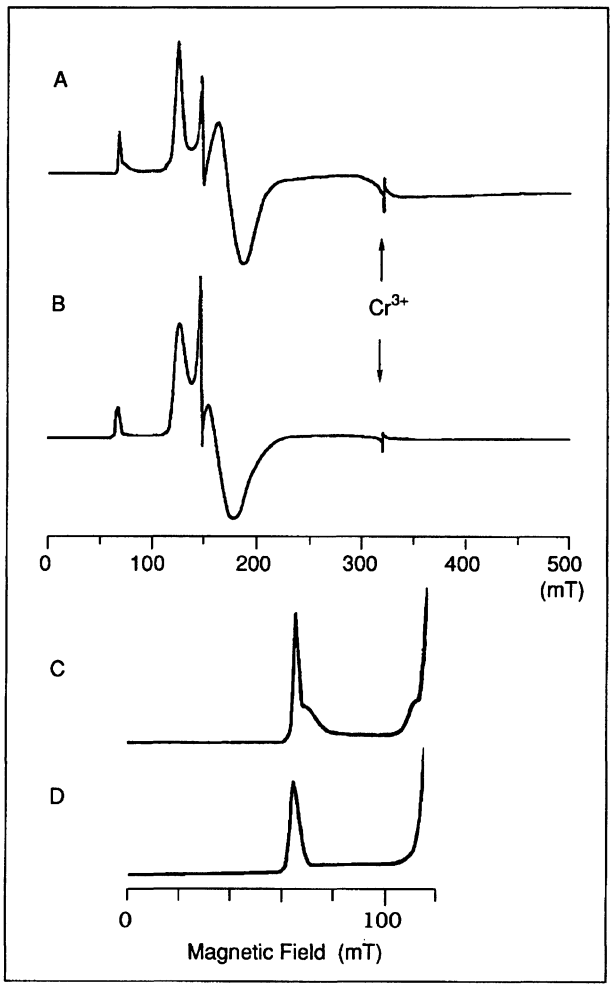

Fig. 2. EPR spectra of (A), (C) $[Fe(nta)(dbc)]^{2-}$ and (B), (D) $[Fe(nta)(pca)]^{2-}$ in DMF/borate buffer (2:1) solution. The spectra (C) and (D) are enlarged spectra of the low field region of (A) and (B), respectively. Spectra at 4.2 K were obtained at 9.18 GHz with 100-kHz modulation.

Table 1. EPR Parameters for Fe(nta)-Catecholate Complexes

Catecholate	g values				E/D (±0.01)
cat	9.10,	5.08,	3.66,	3.32	0.20[a]
4Mecat	9.07,	4.99,	3.68,	3.34	0.20
3Mecat	9.09,	5.07,	3.73,	3.37	0.20
pbc	9.05,	5.00,	3.66,	3.30	0.20[b]
dbc	9.10,	5.08,	3.69,	3.38	0.20[a]
	8.3,	5.4			0.13
pca	9.18,	4.93,	3.88,	3.52	0.22
hpca	9.07,	5.01,	3.70,	3.31	0.20
$4NO_2cat$	9.24,	4.71,		3.65	0.23

a) In Ref. 20, 0.20 and 0.18 are reported for cat and dbc, respectively in DMF/Me_2SO/toluene. b) In Ref. 10b, $E/D=0.24$ is reported for pbc in EtOH/borate buffer.

with eight kinds of catechols (cf. Figs. 2C and 2D). Small signals at $g=8.3$ and 5.4 arise from minor species with $E/D=0.13$. This minor species has a different metal environment from the chelated catecholate one (Type II; $E/D\approx0.20$) and is probably the adduct of the monodentate catecholate dianion (Type III), [Fe(nta)-(dbc)]$^{2-}$, treated later.

The visible spectra of the Fe(nta)-catecholate complexes prepared anaerobically are characterized by two absorption bands (Fig. 3, Table 2). These two bands are assigned to catecholate-to-iron(III) ligand-to-metal charge transfer (LMCT) bands.[14] The lower energy absorption band shifts to higher energy as the nature of the substituents on the catecholate are varied from electron donating to electron withdrawing. However, the spectra of the complexes prepared aerobically exhibit one broad band.

Time-course of the reaction was traced by EPR (Fig. 4). As the reaction with O_2 proceeded, the signal intensity derived from the chelated catecholate complex decreased gradually, followed by the concomitant increase of that of original Fe(nta). From the EPR

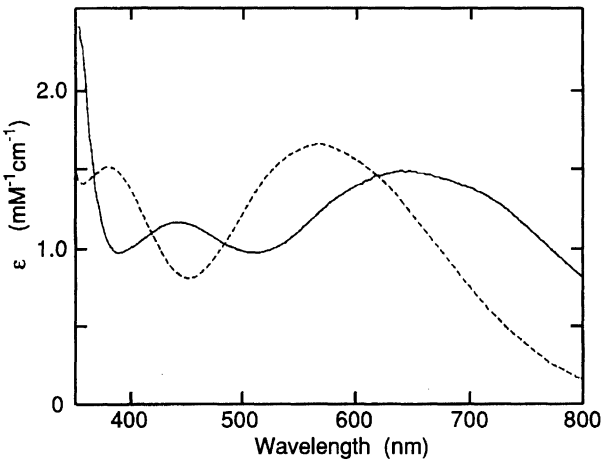

Fig. 3. Visible spectra of [Fe(nta)(dbc)]$^{2-}$ (solid line) and [Fe(nta)(pca)]$^{2-}$ (dashed line). Spectra were obtained anaerobically in DMF/borate buffer (2:1) solution.

Table 2. Catecholate Dependences of Absorption Maxima and Reaction Time of Fe(nta)-Catecholate Complexes in DMF/Borate Buffer Solution

Catecholate	λ_{max} nm		Reaction time (days) R.T.	50 °C
$4NO_2$cat	—	470	>10	>10
pca	379	566	>10	9
hpca	404	580	>10	9
cat	403	584	10	7
3Mecat	408	604	9	7
4Mecat	415	625	9	7
pbc	416	628	10	7
dbc	440	646	7	3

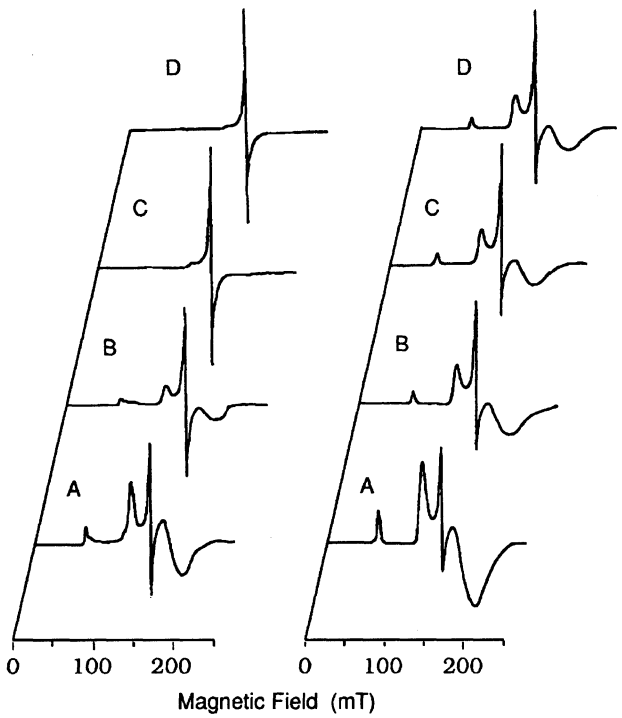

Fig. 4. Time-course of EPR spectra of [Fe(nta)-(dbc)]$^{2-}$ (left) and [Fe(nta)(cat)]$^{2-}$ (right). The spectra were recorded at (A) 1 h, (B) 2 d, (C) 4 d, and (D) 6 d after addition of catechols.

spectra, the chelated dbc complex with $E/D=0.20$ almost disappeared in 6 d (Fig. 4 left). On the other hand, a considerable amount of chelated cat complex with $E/D=0.20$ still remained 6 d later (Fig. 4 right). Neither apparent EPR intensity change indicating the reduction of the iron ion from iron(III) to iron(II) nor signal of an organic free radical was observed during the reaction. These observations suggest that the iron remained in the iron(III) high-spin state and that the reaction time depends on the substrate catechols. Catecholate dependence is also observed in the absorption spectra (vide infra). The absorption band in the visible region also diminished corresponding to the change of EPR. Such intensity changes observed in EPR and absorption spectra could not be seen without O_2. At the initial stage of the reaction, however, identical EPR spectra could be observed regardless of the presence of O_2. It suggests that the formation of the catecholate complexes (ES in Scheme 1) is the first step of the catalytic cycle.

The reaction times with O_2, in which the characteristic LMCT bands had faded, are lised in Table 2. They are consistent with the decay time of the chelated catecholate complexes observed with the EPR (Fig. 4). It is interesting that the reaction time correlates with the nature of the substituents on the catecholate. The catecholate having more electron-donating substituent reacted faster than the one having less electron-donating substituent. It is worth noting that the dbc com-

plex, solely having a minor species with $E/D=0.13$ reacted especially fast. This fact suggests that this minor species, monodentate dianionic catecholate complex with the coordination mode of Type III, plays an important role in the model reaction.

Fe(salen)Cl System. Fe(salen)Cl in MeOH showed an EPR spectrum at $g=4.3$. Fe(salen)Cl and H_2dbc in MeOH did not react without alkaline reagents. Upon anaerobic addition of one or more equiv of *t*-BuOK, the purple of $[Fe(salen)]^+$($\lambda_{max}=510$ nm, not shown) changed to green ($\lambda_{max}=620$ nm). The sharp resonance at $g=4.3$, arising from the original Fe(salen)-Cl, decreased and the new $g=8.75$, 5.10, 3.78, and 3.11 ($E/D=0.19$) resonances appeared. The broad signal at $g=4.3$ ($E/D=0.30$) was also observed (Fig. 5A). This broad spectrum arose from the adduct of the catecholate monoanion, [Fe(salen)(Hdbc)] (Type I).[22] These changes could be observed for the solution prepared aerobically.

When more than twofold excess of *t*-BuOK was added to the Fe(salen)Cl : H_2dbc 1 : 1 solution, the intensity of the chelated catecholate complex decreased extremely and the 3,5-di-*t*-butyl-*o*-semiquinone (DBSQ) radical at $g=2.004$ was observed (Fig. 5B). A similar result could be obtained from the sample prepared anaerobically. These observations indicate the following electron-transfer process:

$$[Fe^{III}(salen)(dbc)]^- \rightarrow Fe^{II}(salen) + DBSQ^- \quad (2)$$

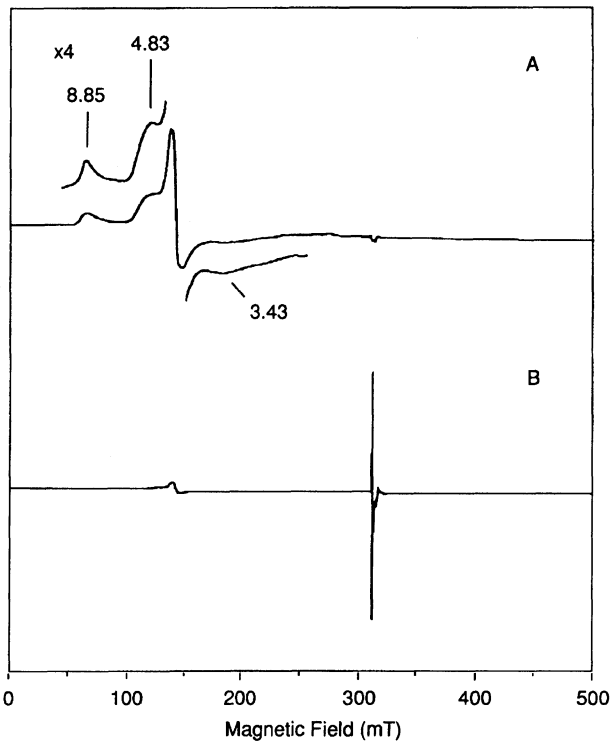

Fig. 5. EPR spectra of (A) $[Fe(salen)(dbc)]^-$ and (B) $Fe^{II}(salen)+DBSQ^-$ in MeOH at 4.2 K. Both samples were prepared anaerobically.

Figure 6 shows the time-course of the EPR and visible absorption spectra. The dashed line in each figure was obtained soon after the addition of *t*-BuOK (Fe : H_2dbc : *t*-BuOK=1 : 1 : 1.5). The EPR spectra with $E/D=0.19$ and the absorption spectra gave their maxima after several minutes and then decreased. Solid lines in each figure show changes after each gave their maxima. These spectral changes indicate that the species with $E/D=0.19$ corresponds to the one with $\lambda_{max}=620$ nm assigned as $[Fe(salen)(dbc)]^-$,[23] where the coordination mode of catecholate is didentate (Type II). There was no time-dependence with the sample prepared anaerobically.

The reaction time of the Fe(salen)Cl system is ca. 2—3 h. The intermediate of Type III structure, which is observed in the Fe(nta) system and gives the great influence on the reaction time, cannot be observed since the iron was reduced to iron(II) state in such a structure.[17]

Fe(sal-L-aa)Cl System. Fe(sal-L-aa)Cl did not react with H_2dbc without alkaline reagents, but the addition of *t*-BuOK gave the catecholate complexes, as was the case of salen complex. Different kinds of catecholate intermediates were generated depending on the amount

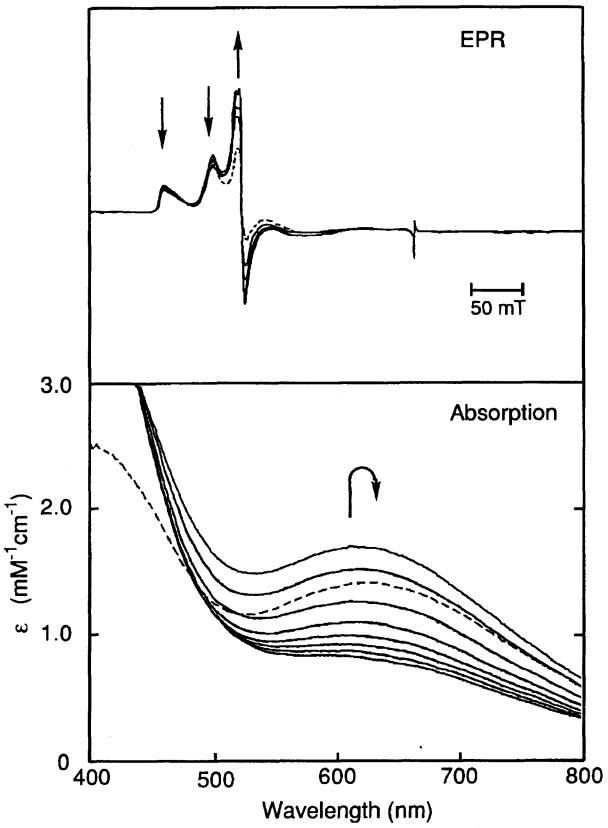

Fig. 6. Time-dependent spectral changes of EPR (top) and visible absorption (bottom) accompanying *t*-BuOK addition (Fe : H_2dbc : *t*-BuOK=1 : 1 : 1.5). Dashed line in each figure is obtained immediately after addition of *t*-BuOK. Successive scans (solid lines) begin 10 min after addition of *t*-BuOK and are 10 min (EPR) and 20 min (visible) apart, respectively.

of the added *t*-BuOK, as was reported by Casella et al.[18] Figure 7 shows, for example, the absorption spectra of Fe(sal-L-val)-catecholate complexes. When *t*-BuOK was added to Fe(sal-L-val)Cl and H_2dbc to give the molar ratio Fe:H_2dbc:*t*-BuOK=1:1:1, Fe(sal-L-val)(Hdbc) was generated (solid line). The transition in the 400—500 nm region is assigned to phenolate to iron(III) LMCT band.[23a] When 2 equiv of *t*-BuOK was added to the Fe(sal-L-val)Cl and H_2dbc 1:1 solution, [Fe(sal-L-val)(dbc)]$^-$ (Type II) was generated and the absorption around 620 nm (dashed line), assigned to catecholate to iron(III) LMCT band, appeared.

EPR spectra of Fe(sal-L-aa)Cl with *t*-BuOK are typical ones for non-heme iron complexes ($E/D\approx1/3$) with peaks at g=9.6 and 4.3 in spite of the difference of the ligand type. Figure 8A shows the EPR spectrum of Fe(sal-L-val)(Hdbc). The same sample was used in the EPR and optical measurements. The spectrum shows two species with main E/D=0.32 (ca. 80%) and minor E/D=0.13 (ca. 20%). Other three sal-L-aa complexes showed similar spectra in spite of the difference, especially for histidine complex (Type **B**), of the ligand structure (Table 3).

EPR spectra of four [Fe(sal-L-aa)(dbc)]$^-$ showed similar features to Fe(sal-L-aa)(Hdbc). However, additional smaller features arising from a trace amount of the chelated catecholate complex ($E/D\approx0.20$) were observed. Main features correspond to the adducts with the catecholate monoanion (Hdbc$^-$; Type I) and minor features to the adducts with the dianion (dbc^{2-}; Type III). The generation of the catecholate dianion species is also supported by the broad features of 600—700 nm, assigned to catecholate to iron(III) LMCT band, in the absorption spectra (Fig. 7 solid line). Although the absorption spectra of Fe(sal-L-aa)(Hdbc) and [Fe(sal-L-aa) (dbc)]$^-$ are different from each other, EPR spectra of both are alike. These observations indicate that the both catecholate complexes have a similar iron environment. Taken together with the optical data, the coordination mode of the dbc^{2-} in minor species should be in a monodentate fashion (Type III, vide infra).

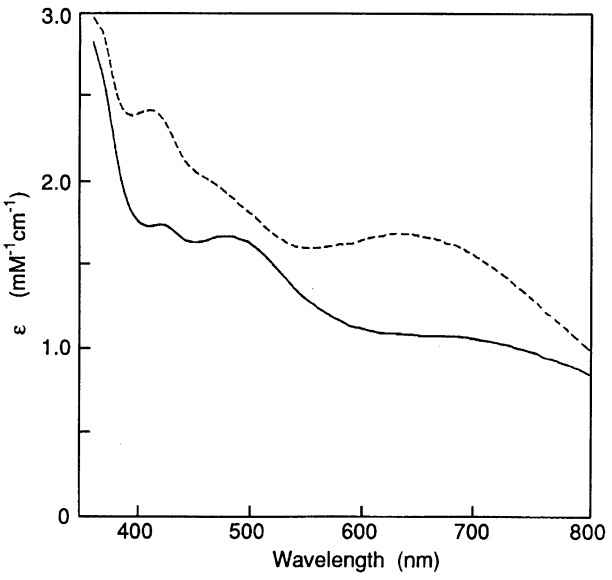

Fig. 7. Visible spectra of Fe(sal-L-val)(Hdbc) (solid line) and [Fe(sal-L-val)(dbc)]$^-$ (dashed line). Spectra were obtained anaerobically in MeOH solution.

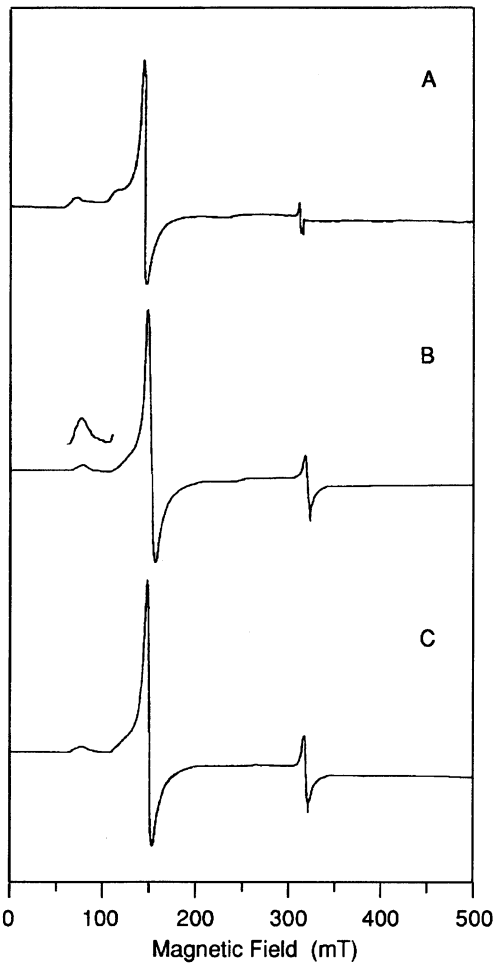

Fig. 8. Progress of reaction of Fe(sal-L-val)DBCH in MeOH with O_2 as monitored by EPR spectroscopy. Spectra were obtained at 0, 20, and 40 min.

The time-courses of EPR and optical spectra for Fe(sal-L-val)(Hdbc) are shown in Fig. 8 (EPR) and Fig. 9 (optical). As the reaction with O_2 proceeded, the adducts of catecholate dianion (Type III; $E/D\approx0.13$) gradually decreased and the uncomplexed [Fe(sal-L-val)]$^+$ increased (Figs. 8B and 8C). No other species could be detected, but sometimes semiquinone radical could be observed (Fig. 8). Since there was no apparent evidence for the iron(III) ion to be reduced in EPR spectra and the signal of the semiquinone radical could not be always detected, the iron ion in this system remained in the iron(III) oxidation state. Absorption spectra measured simultaneously show an interesting behavior (Fig. 9 top). First, the Fe(sal-L-val)(Hdbc) type absorption (solid line) was observed immediately after the

Table 3. EPR and Optical Data for Fe(sal-L-aa)-Catecholate Complexes

Complex	g values			E/D (±0.01)	λ_{max} (nm)
Fe(sal-L-ala)(Hdbc)	4.44,	4.25,	4.11[a)]	0.30	400,466[b)]
[Fe(sal-L-ala)(dbc)]$^-$	8.16,	5.55,		0.11	400,625
Fe(sal-L-val)(Hdbc)	4.46,	4.24,	4.10[a)]	0.30	417,473[b)]
[Fe(sal-L-val)(dbc)]$^-$	8.33,	5.26,		0.13	409,625
Fe(sal-L-phe)(Hdbc)	4.52,	4.20,	3.96[a)]	0.29	414,472[b)]
[Fe(sal-L-phe)(dbc)]$^-$	8.85,	5.37,		0.16	400,628
Fe(sal-L-his)(Hdbc)	4.37,	4.25,	4.14[a)]	0.31	417,470[b)]
[Fe(sal-L-his)(dbc)]$^-$	8.06,	5.60,		0.11	407,645

a) The g value of low field resonance ($g\approx9.5$) could not be obtained due to the broad feature of the species with $E/D\approx0.13$. b) The shoulder observed in 600—700 nm region is not shown.

addition of 1 equiv of t-BuOK. As the reaction with O_2 proceeded, it shifted to the [Fe(sal-L-val)(dbc)]$^-$ type (dashed line), and then decreased gradually (not shown for clarity). These spectral changes clearly showed that the deprotonation from the catecholate monoanion did not affect the iron environment. Thus the minor species with $E/D=0.13$ should be the adducts of catecholate dianion in a monodentate fashion (Type III). When 2 equiv of t-BuOK was added to the reaction mixture, the [Fe(sal-L-val)(dbc)]$^-$ type absorption could be observed immediately and then decreased (Fig. 9 bottom). No time-dependence in EPR and absorption spectra could be observed with samples prepared anaerobically.

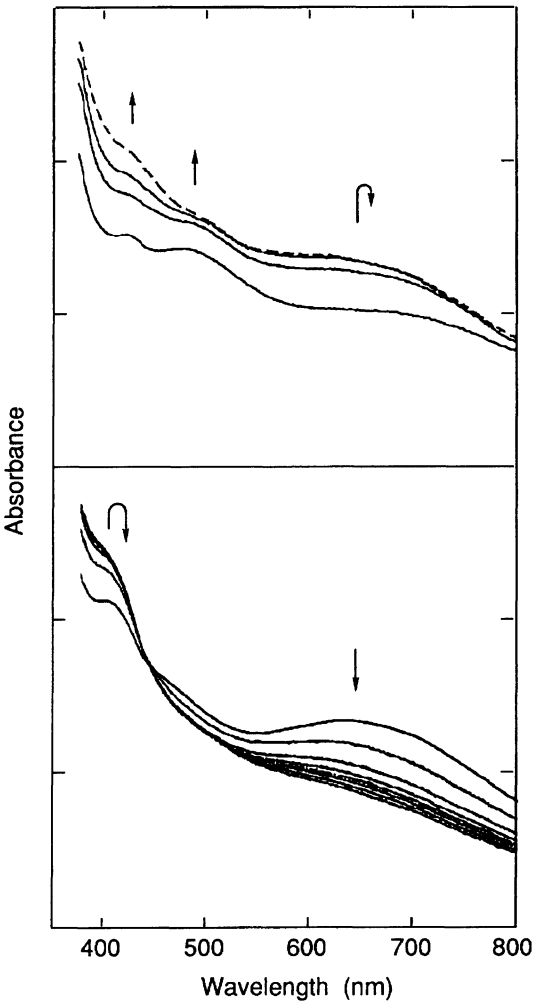

Fig. 9. Time-course of visible spectra of Fe(sal-L-val)-(Hdbc) (top) and [Fe(sal-L-val)(dbc)]$^-$ (bottom) in MeOH. Top: Spectral changes from Fe(sal-L-val)-(Hdbc) type to [Fe(sal-L-val)(dbc)]$^-$ type (dashed line) are shown. Successive scans are 10 min apart. Bottom: Decays of dbc complex are shown. Successive scans are 5 min apart.

The reaction time of the Fe(sal-L-aa)(Hdbc) is ca. 1 h. On the other hand, the reaction time of the [Fe(sal-L-aa)(dbc)]$^-$ is 20—30 min. This difference is due to the deprotonation process of the Fe(sal-L-aa)(Hdbc). In any case, Fe(sal-L-aa)Cl reacts with H_2dbc and O_2 faster than Fe(nta) and Fe(salen)Cl.

Electrochemical Studies. Complexes used in this study were also investigated electrochemically (Table 4). All the complexes except Fe(nta) show a redox process associated with the Fe(III)/Fe(II) couple, which ranges from −93 to −134 mV. For Fe(nta), the redox process could not be observed due to lack of solubility to Me_2SO. In general, the redox potential shifts to more negative values as the electron donating alkyl group in the amino acid becomes large. Moreover, the redox potential shifts to positive values if the ligand has another pπ orbital in addition to the phenolate moiety of salicylaldehyde. From the results of EPR, only salen complex was reduced to iron(II) state. In respect to the facility with reduction, however, the electrochemi-

Table 4. Electrochemical Data for the Model Complexes

Complex	$E^{\circ\prime}$(mV)
Fe(nta)	—[a)]
Fe(salen)Cl	−100
Fe(sal-L-ala)Cl	−122
Fe(sal-L-val)Cl	−134
Fe(sal-L-phe)Cl	−109
Fe(sal-L-his)Cl	−93

a) Fe(nta) was not dissolved in Me_2SO.

cal data show no specialty of salen complex.

Oxygenation Studies. We have investigated products obtained in the oxygenation of H_2dbc (10 equiv) in the presence of *t*-BuOK (10 equiv), and Fe(sal-L-val)Cl (1 equiv) in MeOH (10 mL) under atmospheric pressure of oxygen. Only H_2dbc was used as a substrate because the *t*-butyl groups minimize the side reactions and facilitate the product analysis. The main products isolated by silica-gel chromatography were compounds **1**, **2**, and **3** (Scheme 4). Their structures are determined by ^{1}H NMR. The ^{13}C NMR spectral data of the products are also consistent with the structures. These products are derived from a muconic anhydride, 2,4-di-*t*-butyl-2,4-hexadienedioic anhydride intermediate (**4**), produced by the intradiol dioxygenolysis of the substrate.

Since the preparative reaction was carried out in aqueous MeOH, the same medium as that of the EPR and optical measurements, compound **4** itself could not be isolated, because **4** is susceptible to nucleophiles such as H_2O and MeOH. If H_2O attacks on the less hindered carbonyl in **4** followed by an intramolecular conjugate addition, then 2,4-di-*t*-butyl-4-(carboxymethyl)-2-buten-4-olide (**5**) is obtained. Compound **1** is derived from further oxidation of **5**. The ^{1}H NMR spectrum of a fraction including **1** shows the presence of a small amount of **5**. This would suggest that compound **1** may result from further oxidation of **5** under the condition. However, Funabiki et al.[11] reported that **1** could be a primary product resulting from an extradiol type oxygenation in the $FeCl_3$/bpy/py system. On the other hand, if MeOH attacks, methyl esters are produced. Whether **2** or **3** is yielded depends on the position where the cyclization occurs. In any case, the immediate product is **4**. Besides the main products, **5**, a trace amount of quinone and some unknown products were also yielded. No unreacted H_2dbc were isolated. Although the exact yield of the products due to dioxygenolysis of the aromatic ring could not be calculated because of the polymerization of the products, the total yield of **1**, **2**, and **3** is not less than 80% of the starting H_2dbc. Base can catalyze the oxygenation of H_2dbc.[24] However, since only 1 equiv of *t*-BuOK relative to H_2dbc was added to the reaction mixture, the solution was nearly neutral during the reaction. Moreover, the product composition observed without the iron complex is different from that with the iron complex. Taken together with the EPR results, these observations indicate that Fe(sal-L-val)Cl serves as a highly specific catalyst for the ring cleavage of catechols not involving the redox process of iron ion.

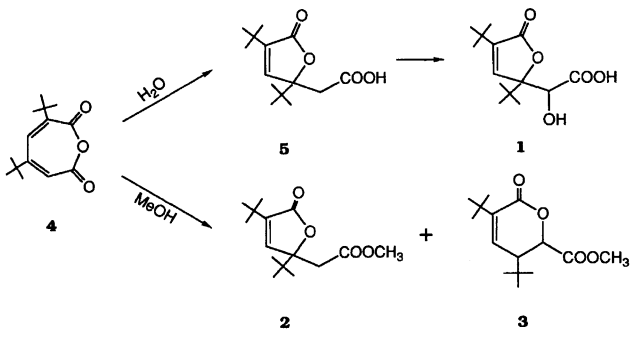

Scheme 4.

2,4-Di-*t*-butyl-4-(1-carboxy-1-hydroxymethyl)-2-buten-4-olide (1): ^{1}H NMR ($CDCl_3$) δ=1.06 (s, 9H), 1.21 (s, 9H), 4.70 (s, 1H), 7.12 (s, 1H); ^{13}C NMR δ=25.9 (q), 28.0 (q), 31.6 (s), 38.0 (s), 77.1 (s), 89.9 (s), 143.2 (s), 145.2 (s), 171.8 (s), 174.7 (s).

2,4-Di-*t*-butyl-4-(methoxycarboxylmetyl)-2-buten-4-olide (2): ^{1}H NMR ($CDCl_3$) δ=0.95 (s, 9H), 1.22 (s, 9H), 2.79 (d, J=14.1 Hz, 1H), 2.93 (d, J=14.1 Hz, 1H), 3.57 (s, 3H), 3.96 (s, 1H).

2,4-Di-*t*-butyl-5-(methoxycarboxyl)-2-penten-5-olide (3): ^{1}H NMR ($CDCl_3$) δ=1.04 (s, 9H), 1.19 (s, 9H), 3.16 (d, J=7.83 Hz, 1H), 3.70 (s, 3H), 4.69 (d, J=7.83 Hz, 1H), 7.09 (s, 1H); ^{13}C NMR ($CDCl_3$) δ=25.8 (q), 28.1 (q), 31.7 (s), 38.0 (s), 53.1 (s), 73.0 (s), 89.3 (s), 139.7 (s), 144.4 (s), 170.7 (s), 173.2 (s).

Discussion

We have investigated the CTD model reactions utilizing Fe(nta), Fe(salen)Cl, and Fe(sal-L-aa)Cl as catalyst. EPR parameters and reaction times of typical catecholate complexes are shown in Table 5. From a perusal of the Tables 1, 3, and 5, it is clear that the values of E/D, a measure of the departure of the electronic environment of the iron from axial symmetry, concentrate on the three distinct ranges, ca. 0.30, ca. 0.20, ca. 0.12. Furthermore, these three correspond to the modes of the catecholate coordination, i.e. monoanionic catecholate (ca. 0.30; Type I), chelated catecholate (ca. 0.20; Type II), and monodentate dianionic catecholate (ca. 0.12; Type III), respectively, as described in the results section. For the reaction of Fe(nta) with H_2dbc, the Type II is observed as a major intermediate along with a trace amount of Type III, only Type II with other catecholates. For Fe(salen)Cl, they are comparable amount of Type I and Type II, and iron(II)-semiquinone species. For Fe(sal-L-aa)Cl, major Type I and minor Type III are observed.

Among three types of catecholate coordination

Table 5. Relation between EPR Parameters and Reaction Time

Complex	E/D	Ratio (%)	Reaction time
$[Fe(nta)(dbc)]^{2-}$	0.20	ca.95	7 d
	0.13	ca.5	
$[Fe(nta)(cat)]^{2-}$	0.20	ca.100	10 d
Fe(salen)(Hdbc)	0.30	ca.50	2—3 h
$[Fe(salen)(dbc)]^{-}$	0.19	ca.50	
Fe(sal-L-val)(Hdbc)	0.30	ca.80	30—60 min
$[Fe(sal\text{-}L\text{-}val)(dbc)]^{-}$	0.13	ca.20	

modes, the Types I and II were confirmed by X-ray crystallography. The crystal of Fe(saloph)(Hcat) (saloph: *N*,*N*′-(1,2-phenylene)bis(salicylideneaminato)) shows square-pyramidal geometry with monoanionic monodentate catecholate (Type I).[25] On the other hand, K[Fe(salen)(cat)][26] and $(dabcoH)_2$[Fe(nta)(dbc)][14] (dabco: 1,4-diaza-bicyclo[2.2.2]octane) are six-coordinate high-spin iron(III) complexes with chelated catecholates (Type II). We have assigned the structures of Types I, II, and III for the species with $E/D \approx 0.30$, ≈ 0.20, and ≈ 0.12, respectively. These assignments are also supported by the following observations. The EPR spectrum of $(dabcoH)_2$[Fe(nta)(dbc)] in DMF/Me_2SO/toluene frozen glass[20] shows similar features to our spectrum of $[Fe(nta)(dbc)]^{2-}$ generated from Fe(nta)$(H_2O)_2$ with H_2dbc in a DMF/borate buffer; thus, the species with $E/D \approx 0.20$ certainly corresponds to the didentate catecholate complex. Fe(salen)(Hdbc), generated from ligand exchange of Fe(salen)OAc (OAc: acetato) with excess H_2dbc,[23] exhibits the broad features at $g=4.3$ ($E/D \approx 0.30$; not shown). Unfortunately, there is no method for generating the species of Type III structure certainly. However, considering the EPR change from Fe(sal-L-aa)(Hdbc) to $[Fe(sal\text{-}L\text{-}aa)(dbc)]^-$, it is most likely that the species with $E/D \approx 0.12$ will have the Type III structure. Such structure is expected to be stabilized by polar solvents such as DMF and MeOH used in this study. From the CD studies,[18] it is suggested that the complexes with Type **A** ligand of sal-L-aa can provide two coordination sites (one axial and one equatorial) that can be occupied by an additional ligand and that the catecholate binds to the iron ion in a didentate mode. Our EPR results, however, indicate the monodentate binding of catecholate dianion.

EPR spectra of enzyme-substrate and enzyme-inhibitor complexes have been reported. For example, the parameters are $E/D=0.02$ and 0.12 for PCD-pca (substrate) complex,[9] $E/D=0.02$ and 0.33 for PCD-hpca (show substrate) complex,[27] and $E/D=0.32$ and 0.24 for PCD-4-hydroxybenzoic acid (inhibitor) complex.[27] Orville and Lipscomb[27] proposed a monodentate catecholate structure for the species with $E/D=0.02$. The E/D values of enzymes and model complexes cannot be compared indiscriminately because of the difference of the ligand flexibility to the exogenous catecholate or O_2 binding. In fact, PCD-substrate complex gives new species when O_2 is introduced,[9] while the model complexes give no new one. However, there is the tendency that plural species are generated in both cases. In the cases of our model systems, it is confirmed by EPR that there are three types of intermediates, monodentate monoanionic catecholate complex (Type I, $E/D \approx 0.30$), didentate catecholate one (Type II), and monodentate monoanionic catecholate one (Type III), in the reaction mixtures.

These structural data taken together with the reaction time afford interesting insights into the mechanism of the CTD-like reaction. The more stable chelated catecholate complex results in the slower reaction with O_2. Conversely, the reaction proceeds fast as the ratio of the Type III intermediate becomes high. These relation indicate that the chelated catecholate intermediate (Type II) is the inactive species, and that monodentate dianionic catecholate intermediate (Type III) is the one reactive toward O_2. Que and co-workers[12,14,16] reported the correlation between the rate of the reaction and the Lewis acidity of the iron(III) center. Our results demonstrate that the structure of the dominant intermediate also affects the reaction rate of oxygenation of catechols.

On the basis of our results, we propose a mechanism for the CTD-like reaction catalyzed by Fe(sal-L-aa)Cl (Scheme 5). In this mechanism, the substrate H_2dbc first coordinates to the iron(III) ion in a monodentate fashion as $Hdbc^-$ form, and then loses another proton. Since each sample prepared aerobically or anaerobically gives similar EPR spectrum until this stage of the reaction, the Type III intermediate may generated independent of the presence or absence of oxygen. The carbanion resulting from the tautomerization of the Type III intermediate reacts with O_2 to produce a peroxide complex, which then decomposes to compound **4**. The deprotonation process of the iron-bound catecholate is clearly demonstrated by the changes in the absorption spectra (Fig. 9 top). In this process, the iron(III) center seems to serve as a promoter of deprotonation of catecholate monoanion, $Hdbc^-$. It is conceivable that this function is attributed to the Lewis acidity of the iron(III) center. However, such apparent spectral changes could not be observed when Fe(sal-L-aa)(Hdbc) was prepared anaerobically; therefore, dioxygen may be participated in this process. The peroxide complex is indispensable for the oxygenation reaction.[28,29] Such a peroxide complex was crystallized in the case of the oxygenation of 2,4,6-tri-*t*-butylphenol by Co(salpr) (salpr: *N*,*N*′-propylbis(salicylideneaminato)).[29b] Recently, the crystal structure of iridium(III)-catecholate peroxide complex was reported as a CTD model.[30] In the oxygenation of catechols, the Lewis acidity of the end of the peroxide bound to the root of a hydroxyl of a catechol affects the mode of oxygenation. Strong Lewis acidity leads to the intradiol cleavage products, on the other hand, weak Lewis acidity does the extradiol ones.[31] This is consistent with the results reported by Que et al. that the yield of the intradiol products increased as the Lewis acidity of the metal center increased.[14] Thus, at this stage of the reaction, iron(III) is favorable.

The above-mentioned mechanism is similar to that proposed previously[14] except for the intervention of the chelated catecholate complex during the catalytic cycle. The virtue of the Fe(sal-L-aa)Cl system is that there is little, if any, amount of the chelated catecholate complex; thus, the monodentate species are predominant. The monodentate coordination of the catecholate facil-

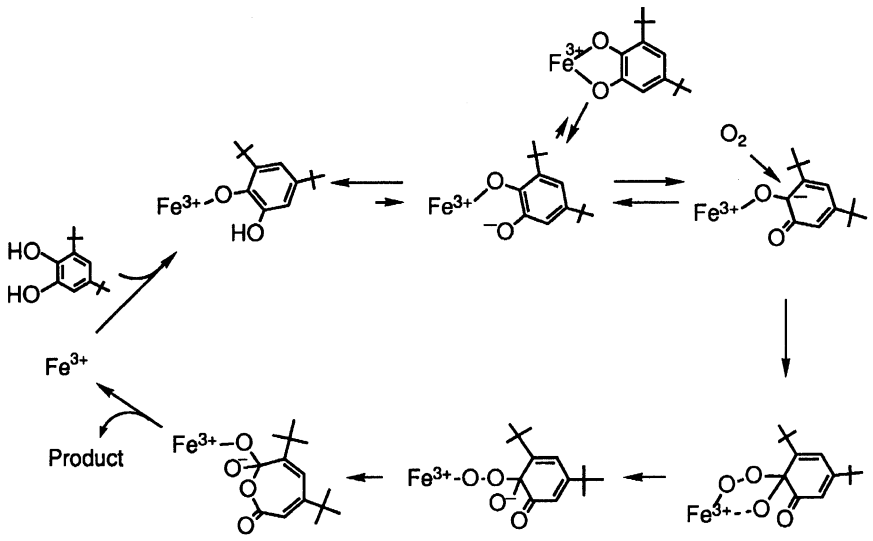

Scheme 5.

itates a keto-enol-like tautomerization of the catecholate to provide an available coordination site for the formation of the peroxide complex. For the Fe(nta) and Fe(salen)Cl systems where the chelated catecholate intermediate is the dominant species, the dissociation of one catecholate oxygen from the iron(III) ion is required to form the peroxide complex. Consequently, the reaction of [Fe(sal-L-aa)(dbc)]$^-$ with O_2 would proceed faster than that of other two substrate complexes.

Taken the intensity changes in the EPR spectra and the observations of organic radicals into consideration, the iron center retains the iron(III) state throughout the reaction utilizing the Fe(nta) and the Fe(sal-L-aa)Cl systems, whereas with the Fe(salen)Cl system the iron(III) center is reduced to the iron(II) state during the reaction. Presumably, O_2 reacts with the iron(III)-catecholate carbanion species in the former case, while with the iron(II)-semiquinonate species in the latter case. In the Fe(salen)Cl system, however, the Type III intermediate, which is probably the reactive species toward O_2 in this system, could not be observed because the reduction of the iron(III) ion may take place during the structural change from the Type II to the Type III.[17] The reduction of the iron(III) center unique to the salen complex may be attributed to the effect of the ligand distortion. The cyclic voltammograms of all the model complexes used in this study show the redox couple (Fe(III)/Fe(II)) near -110 mV (Table 4). Since salen is a planar ligand having two phenolate $p\pi$ orbitals overlapped directly with the $d\pi$ orbitals in the iron(III) ion, catecholate coordination in a didentate mode is expected to distort the ligand and to affect the redox potential of iron in [Fe^{III}(salen)]$^+$; indeed, the crystal of [Fe(salen)(cat)]$^-$ exhibits the distorted octahedral structure with the distorted salen ligand.[26]

Recently, Funabiki et al.[32] and Que et al.[16] reported that the bound catecholate had a strong radical character and proposed the iron(II)-semiquinone intermediate as a reactive species toward dioxygen. Both groups deduced their conclusion from the NMR downfield shifts of the catecholate ligand. Funabiki et al. also reported that the equivalents of Fe(II) and Fe(III) were observed in the Mössbauer spectrum on the $FeCl_3$/bpy/py-H_2dbc system.[15b] On the contrary, Mössabauer[5—7] and EPR[5—7,9,27] studies of enzyme-substrate complexes indicate the iron(III)-catecholate species. Our results obtained from the present model studies suggest that both are probable candidates for a reactive species toward O_2, i.e. the iron(III)-catecholate species for Fe(nta) and Fe(sal-L-aa)Cl, and the iron(II)-semiquinonate species for Fe(salen)Cl. Even in the Fe(nta) and the Fe(sal-L-aa)Cl systems, it is conceivable that only a few amounts of iron(II)-semiquinonate species are generated, because it is difficult to judge such a thing from EPR or other spectroscopies. However, taken the resultant products into consideration, iron(III)-catecholate species is more likely. Fe(nta)[10,14] and Fe(sal-L-aa)Cl give a ca. 80% yield of the ring cleavage products, while Fe(salen)Cl, where the iron(II)-semiquinonate is probably a reactive species toward O_2, gives a ca. 30% yield.[14] Even being subtracted the effect of the side reaction of Fe(salen)(Hdbc) with O_2,[23a] the salen complex would be a less efficient catalyst than other two complexes. Further information about the products yields by iron(II) species was reported by Funabiki et al.[11] In the $FeCl_3$/bpy/py system, where the presence of equimolar amounts of Fe(II) and Fe(III) are observed, the main product (50—70%) is 3,5-di-*t*-butyl-1,2-benzoquinone and the total yields of the ring cleavage products is less than 50%. An interesting relation is also pointed out by Cox and Que:[12] The relation which stronger semiquinone character of iron-bound catecholate brings less specificity for intradiol cleavage. Although all the factors of these less

specificity toward the ring cleavage products could not be ascribed to the iron(II)-semiquinone species, there seems some relation between the yields of the ring cleavage products and the iron(II)-semiquinone intermediate. Although our EPR and optical results, of course, cannot definitely exclude the possibility that the iron(III)-catecholate species has the iron(II)-semiquinone character, we prefer the iron(III)-catecholate intermediate from these considerations.

In conclusion, we have investigated the structures of the intermediates appeared in the CTD model systems. There are three types of intermediates which have different coordination modes of the catecholate. Among these three, the iron(III)-monodentate dianionic catecholate (Type III) is most probable as the direct reactant with O_2. In enzyme systems, the participation of the chelated catecholate in the catalytic cycle has been proposed by EPR[27] and EXAFS[33] studies. In the case of Fe(sal-L-aa)Cl, however, the chelated catecholate species (Type II) could not be detected. It is a novel point of this system. In order to elucidate the reaction mechanism of the Fe(sal-L-aa)Cl system, further systematic investigations are now under way.

Correlation between the EPR Parameters and the Envionment of the Non-Heme Iron(III) Ion. The typical EPR spectrum observed at $g=4.3$ for the high-spin non-heme iron(III) ion has been interpreted by spin Hamiltonian (Eq. 1) since Castner et al.[34] succeeded in the explanation of its origin. Since then, a lot of theoretical studies have been made to explain the observed g values of non-heme iron(III) ions under various environments.[35—41] Essentially, as described in the results section, the observed g values of non-heme iron(III) ions only depend upon the E/D (Fig. 1) due to the three Kramers doublets at zero field. The E/D reflects the iron envionment and can be represented on the interval $0 \leq E/D \leq 1/3$.[42] $E/D=0$ corresponds to the axial symmetry, which shows $g=6$ and 2 resonances, and $E/D=1/3$ to the rhombic symmetry, which shows $g=4.3$ resonance. Despite a variety of coordination environments, almost non-heme iron complexes and enzymes show the EPR spectra at $g=4.3$ with $E/D \approx 1/3$ in their resting states. However, the spectra change with the coordination of exogenous ligands to the iron(III) center. Typical examples are shown in Figs. 2A and 2B. Unfortunately, there have been no relation between the observed g values and the coordination environments of non-heme iron(III) complexes and enzymes. Consequently, one has not been able to derive the information on the coordination environments of the iron(III) center directly from the EPR spectra of non-heme iron(III) complexes and enzymes. These contrast to the cases of heme complexes and enzymes where the axial ligands can be deduced from the parameters tetragonality and rhombicity calculated from the observed g values.[43] Therefore, another purpose of our studies is to examine whether there is such a relation or not in the case of the non-heme iron complexes and enzymes.

In the course of our investigation of the reactions of non-heme iron(III) complexes with various substrates, we have found an interesting tendency of the EPR spectra. As discussed in the CTD model studies, monoanionic monodentate catecholate complexes show the EPR spectra with $E/D \approx 0.30$, dianionic didentate catecholate complexes with $E/D \approx 0.20$, and dianionic monodentate catecholate complexes with $E/D \approx 0.12$. Other examples are Fe(III)(edta) peroxide complexes (edta: ethylenediaminetetraacetato).[44] The monodentate peroxide complexes, Fe^{III}(edta)-$^{-}$OOR (R=H, *n*-butyl, and *t*-butyl), exhibit the EPR spectra with $E/D \approx 0.30$, and the didentate peroxide complex, Fe^{III}(edta)-O_2^{2-}, exhibits with $E/D \approx 0.20$. The iron(III)-peroxide complexes of edta derivatives also show similar behavior.[45] Phenolate coordination to the non-heme iron(III) complexes used in these studies gives the EPR spectrum with $E/D \approx 0.30$. Our observations indicate a correlation between the E/D estimated from the observed g values and the number of exogenous oxyanion ligands, i.e., $E/D \approx 0.30$ for one exogenous oxyanion ligand, $E/D \approx 0.20$ for two exogenous ones both of which bind to the iron(III) center, and $E/D \approx 0.12$ for two exogenous ones one of which, however, is in the proximity of the iron(III) center but not bind to it (Type III conformation in CTD models). Unfortunately, this correlation cannot apply to other exogenous ligands such as nitrogen; indeed, pyridine or bipyridine coordination gives entirely different tendencies. This is explained qualitatively as follows. The D and E are ligand field parameters which include the effects of ligands electrostatically. Accordingly, it is natural that the influence given by an anionic oxygen should be different from that given by neutral nitrogen. It is also the case with the number of exogenous oxyanion ligands. Probably the conformation corresponding to $E/D \approx 1/3$ is most stable for the non-heme iron complexes in solution and for most of the non-heme iron enzymes. When the exogenous oxyanion binds to the iron(III) center, the conformation of the original ligands would change to a new stable state. In this point, there will be a difference between complexes and enzymes due to the difference of the flexibility of the original ligands. As a consequence, this correlation does not always apply to the enzyme systems. However, we think it a clue to an exploration into the more general correlation between the coordination environments of the non-heme iron ions and the EPR parameters.

We thank Mr. Kazushige Maruyama of Osaka Institute of Techonology for the measurements of NMR spectra. This work is partially supported by the Grant-in-Aid for Scientific Research from the Ministry of Education, Science and Culture.

References

1) M. Nozaki, "Molecular Mechanisms of Oxygen Activation," ed by O. Hayaishi, Academic Press, New York and London (1974).

2) a) L. Que, Jr., *Adv. Inorg. Biochem.*, **5**, 167 (1983); b) L. Que, Jr., *J. Chem. Educ.*, **62**, 938 (1985).

3) D. H. Ohlendorf, J. D. Lipscomb, and P. C. Weber, *Nature*, **336**, 403 (1988).

4) C. Bull, D. P. Ballou, and S. Ohtsuka, *J. Biol. Chem.*, **256**, 12681 (1981).

5) L. Que, Jr., J. D. Lipscomb, R. Zimmermann, E. Münck, N. R. Orme-Johnson, and W. H. Orme-Johnson, *Biochim. Biophys. Acta*, **452**, 320 (1976).

6) J. W. Whittaker, J. D. Lipscomb, T. A. Kent, and E. Münck, *J. Biol. Chem.*, **259**, 4466 (1984).

7) T. A. Kent, E. Münck, J. W. Pyrz, J. Widom, and L. Que, Jr., *Inorg. Chem.*, **26**, 1402 (1987).

8) T. A. Walsh, D. P. Ballou, R. Mayer, and L. Que, Jr., *J. Biol. Chem.*, **258**, 14422 (1983).

9) L. Que, Jr., J. D. Lipscomb, E. Münck, and J. M. Wood, *Biochim. Biophys. Acta*, **485**, 60 (1977).

10) a) M. G. Weller and U. Weser, *J. Am. Chem. Soc.*, **104**, 3752 (1982); b) M. G. Weller and U. Weser, *Inorg. Chim. Acta*, **107**, 243 (1985).

11) T. Funabiki, A. Mizoguchi, T. Sugimoto, S. Tada, M. Tsuji, H. Sakamoto, and S. Yoshida, *J. Am. Chem. Soc.*, **108**, 2921 (1986).

12) D. D. Cox and L. Que, Jr., *J. Am. Chem. Soc.*, **110**, 8085 (1988).

13) Y. Nishida, K. Yoshizawa, S. Takahashi, and I. Watanabe, *Z. Naturforsch., C*, **47C**, 209 (1992).

14) L. Que, Jr., R. C. Kolanczyk, and L. S. White, *J. Am. Chem. Soc.*, **109**, 5373 (1987).

15) a) T. Funabiki, H. Sakamoto, S. Yoshida, and K. Tarama, *J. Chem. Soc., Chem. Commun.*, **1979**, 754; b) T. Funabiki, S. Tada, T. Yoshioka, M. Takano, and S. Yoshida, *J. Chem. Soc., Chem. Commun.*, **1986**, 1699; c) T. Funabiki, T. Konishi, S. Tada, and S. Yoshida, *Chem. Lett.*, **1987**, 1803.

16) H. G. Jang, D. D. Cox, and L. Que, Jr., *J. Am. Chem. Soc.*, **113**, 9200 (1991).

17) S. Fujii, H. Ohya-Nishiguchi, and N. Hirota, "Dioxygen Activation and Homogenous Catalytic Oxidation," ed by L. I. Simándi, Elsevier, Amsterdam (1991), p. 321.

18) L. Casella, M. Gullotti, A. Pintar, L. Messori, A. Rockenbauer, and M. Györ, *Inorg. Chem.*, **26**, 1031 (1987).

19) M. Gerloch and F. E. Mabbs, *J. Chem. Soc. A*, **1967**, 1900.

20) D. D. Cox, S. J. Benkovic, L. M. Bloom, F. C. Bradley, M. J. Nelson, L. Que, Jr., and D. E. Wallick, *J. Am. Chem. Soc.*, **110**, 2026 (1988).

21) It was confirmed by controlling the amount of the added catechol. The $g=4.3$ signal is getting smaller as the amount of the added catechol is increasing.

22) It was verified by measuring the Fe(salen)(Hdbc) generating by another method (see Discussion).

23) a) R. B. Lauffer, R. H. Heistand, II, and L. Que, Jr., *J. Am. Chem. Soc.*, **103**, 3947 (1981); b) R. H. Heistand, II, R. B. Lauffer, E. Fikrig, and L. Que, Jr., *J. Am. Chem. Soc.*, **104**, 2789 (1982).

24) a) V. H. Schulze and W. Flaig, *Justus Liebigs Ann. Chem.*, **573**, 231 (1952); b) R. R. Grinstead, *Biochemistry*, **3**, 1308 (1964); c) F. R. Hewgill and S. L. Lee, *J. Chem. Soc. C*, **1969**, 2080; d) A. Nishinaga, T. Itahara, and T. Matsuura, *Bull. Chem. Soc. Jpn.*, **47**, 1811 (1974).

25) R. H. Heistand, II, A. L. Roe, and L. Que, Jr., *Inorg. Chem.*, **21**, 676 (1982).

26) R. B. Lauffer, R. H. Heistand, II, and L. Que, Jr., *Inorg. Chem.*, **22**, 50 (1983).

27) A. M. Orville and J. D. Lipscomb, *J. Biol. Chem.*, **264**, 8791 (1989).

28) a) S. Muto and T. C. Bruice, *J. Am. Chem. Soc.*, **102**, 7559 (1980); b) S. Muto and T. C. Bruice, *J. Am. Chem. Soc.*, **104**, 2284 (1982).

29) a),A. Nishinaga, H. Tomita, T. Shimizu, and T. Matsuura, *J. Am. Chem. Soc.*, **100**, 1821 (1978); b) A. Nishinaga, H. Tomita, K. Nishizawa, T. Matsuura, S. Ooi, and K. Hirotsu, *J. Chem. Soc., Dalton Trans.*, **1981**, 1504.

30) P. Barbaro, C. Bianchini, C. Mealli, and A. Meli, *J. Am. Chem. Soc.*, **113**, 3181 (1991).

31) a) A. Nishinaga, *Kagaku*, **38**, 740 (1983); b) A. Nishinaga, "A Book of Abstract. The 1984 International Chemical Congress of Pacific Basin Societies," 04B04 (1984).

32) T. Funabiki, H. Kojima, M. Kaneko, T. Inoue, T. Yoshioka, T. Tanaka, and S. Yoshida, *Chem. Lett.*, **1991**, 2143.

33) A. E. True, A. M. Orville, L. L. Pearce, J. D. Lipscomb, and L. Que, Jr., *Biochemistry*, **29**, 10847 (1990).

34) T. Castner, Jr., G. S. Newell, W. C. Holton, and C. P. Slichter, *J. Chem. Phys.*, **32**, 668 (1960).

35) a) J. S. Griffith, *Mol. Phys.*, **8**, 213 (1964); b) J. S. Griffith, *Mol. Phys.*, **8**, 217 (1964).

36) H. H. Wickman, M. P. Klein, and D. A. Shirley, *J. Chem. Phys.*, **42**, 2113 (1965).

37) M. Gerloch, J. Lewis, and R. C. Slade, *J. Chem. Soc. A*, **1969**, 1422.

38) R. D. Dowsing and J. F. Gibson, *J. Chem. Phys.*, **50**, 294 (1969).

39) R. Aasa, *J. Chem. Phys.*, **52**, 3919 (1970).

40) G. Lang, R. Aasa, K. Garbett, and R. J. P. Williams, *J. Chem. Phys.*, **55**, 4539 (1971).

41) W. V. Sweeney, D. Coucouvanis, and R. E. Coffman, *J. Chem. Phys.*, **59**, 369 (1973).

42) W. E. Blumberg, "Magnetic Resonance in Biological Systems," ed by A. Ehrenberg, B. G. Malmstrom, and T. Vänngard, Pergamon Press, New York (1967), p. 119.

43) W. E. Blumberg and J. Peisach, *Adv. Chem. Ser.*, **100**, 271 (1971).

44) S. Fujii, H. Ohya-Nishiguchi, and N. Hirota, *Inorg. Chim. Acta*, **175**, 27 (1990).

45) S. Fujii, H. Ohya-Nishiguchi, and N. Hirota, in preparation.